Regular Article

PHYSICAL CHEMISTRY RESEARCH
Published by the
Iranian Chemical Society
www.physchemres.org
info@physchemres.org

Phys. Chem. Res., Vol. 10, No. 3, 391-409, September 2022
DOI: 10.22036/PCR.2022.317494.1996

Modified Thymidine Derivatives as Potential Inhibitors of SARS-CoV: PASS, *In Vitro* Antimicrobial, Physicochemical and Molecular Docking Studies

A. Alam[a], K.M. Rana[a], M.A. Hosen[a], S. Dey[b], B. Bezbaruah[c] and S.M.A. Kawsar[a,*]

[a]*Laboratory of Carbohydrate and Nucleoside Chemistry, Department of Chemistry, Faculty of Science, University of Chittagong, Chittagong-4331, Bangladesh*

[b]*Department of Microbiology, Faculty of Biological Science, University of Chittagong, Chittagong-4331, Bangladesh*

[c]*Department of Applied Sciences, Gauhati University, Guwahati-781014, Assam, India*

(Received 29 November 2021, Accepted 2 February 2022)

Thymidine and thymidine-mimicking derivatives were found to be promising agents against some microorganisms that inhibited the growth of other microorganisms providing effective therapies for several diseases. In the present study, the antimicrobial activities of thymidine and some of its designed derivatives were investigated by employing quantum chemical calculations to assess their thermodynamic and other biochemical parameters. The antimicrobial tests demonstrated that compounds 3, 4, and 14 were the most active against *Pseudomonas aeruginosa*, *Salmonella abony*, and *Staphylococcus aureus* strains, with the calculated minimum inhibitory concentration (MIC) values ranging from 0.32 ± 0.01 to 1.25 ± 0.03 mg ml^{-1} and minimum bactericidal concentration (MBC) values ranging from 0.32 ± 0.01 to 2.5 ± 0.06 mg ml^{-1}. These derivatives exhibited much stronger biochemical activities than the standard antibacterial drugs. A structure-activity relationship (SAR) study, including *in vitro* and *in silico* analysis, revealed that the acyl groups, lauroyl (C12), and myristoyl (C14), in combination with ribose sugar, had the most potent activity against human and fungal pathogens. Prediction of activity spectra for substances (PASS) and quantum calculations, respectively, revealed excellent antimicrobial and thermodynamic properties of the designed thymidine derivatives. A molecular docking study was performed against SARS-CoV main protease protein to investigate its binding energy and binding mode. The designed derivatives exhibited improved binding affinities compared to the parent ligand thymidine. In addition, the ADMET (absorption, distribution, metabolism, elimination, toxicity) studies predicted the pharmacokinetic properties with lower acute oral toxicity, *i.e.*, non-carcinogenic effects of all compounds.

Keywords: Thymidine, Antibacterial, Antifungal, Quantum calculations, Molecular docking, SARS-COV M^{pro}

INTRODUCTION

Nucleoside analogs (NAs) are the subunits of DNA and RNA and consist of a sugar moiety connected to a nitrogen base through an *N*-β-glycosidic bond [1]. NAs have immense clinical importance as medicinal agents and, due to their antiviral and anticancer activities [2], have been the drugs of choice for the prevention of various viral infections, such as herpes simplex (HSV-1), human cytomegalovirus, varicella-zoster, human immunodeficiency virus (HIV) type-1, human hepatitis B (HBV) and C (HCV) [3], Ebola [4], dengue [5], and Zika [6]. In addition, 2′-deoxynucleosides, such as doxuridne, trifluridine, doxudine, vidarabine, and brivudine, have been used for the treatment of herpes virus infections [7,8]. Certain 2′,3′-dideoxynucleosides, such as zidovudine, didanosine, zalcitabine, stavudine, and abacavir, have been shown to be the most promising therapeutic candidates against HIV [9]. The modifications in the sugar moiety (*i.e.*, ribofuranose or deoxyribofuranose) of nucleosides were done with changes in the sugar substituents, alteration of the oxygen with another atom, insertion of the heteroatom in

*Corresponding author. E-mail: akawsarabe@yahoo.com

the sugar ring, ring size variations, and replacement with an acyl group. Such arrangements may bring notable variations in the biological activity and degree of selective toxicity depending on the respective chemical and physical properties. The designed compounds exhibited a broad-spectrum biological activity. For example, zidovudine with azido group at the 3′-position was used for the treatment of HIV infection. Thymidine (1) derivatives, such as telbivudine, are used as antiviral drugs in the treatment of HBV [10]. Azidothymidine (3′-azido-2′,3′-dideoxythymidine) is also a thymidine analog used in the treatment of HIV. A carbocyclic analog of thymidine showed significant activity against leukemia L1210 cell lines, as well as HSV-1, with an MIC_{50} value of 0.8μg/ml [11]. Thymidine derivatives, such as stavudine and zalcitabine, have been shown to be effective in the treatment of HIV infections and tumors [12]. Antimicrobial agents have been used to treat diseases caused by various microorganisms for a long time. However, the overuse of antimicrobial agents will ultimately result in drug-resistant microorganisms [13]. Except for a few antibiotics such as erythromycin and vancomycin, microorganisms show a unique resistance against the majority of antibiotics. To mitigate these problems, researchers around the world are searching for novel agents that are less toxic, better tolerated by patients, and more effective in combating microorganisms [14]. Many medicinal scientists have focused on compounds having aromatic heterocyclic rings with nitrogen atoms in their structure. Antimicrobial screening of the nucleosides that have been related to selective acylation methods revealed that nitrogen-, sulfur-, and halogen-bearing substituted products had significantly higher antimicrobial and biological activities than their parent compounds [15]. A novel coronavirus disease (COVID-19), associated with a severe acute respiratory syndrome (SARS) started in Wuhan, China, is spreading rapidly in humans and is now considered a global pandemic [16]. Modifications of the hydroxyl (-OH) group of nucleoside structure revealed some potent anti-SARS-CoV-2 candidates [17] and antimicrobial agents [18]. Though SARS-CoV and SARS-CoV-2 agents belong to the beta-coronaviruses category, they are slightly different from each other. Recent research has shown that SARS-CoV-2 often shares 80% nucleotide identity and 89.1% nucleotide similarity with SARS-CoV. Thus, the main protease of SARS-CoV, $3CL^{pro}$ has been the target of several *in silico* investigations to develop potential inhibitors. The $3CL^{pro}$ has a high sequence identity rate between nCoV and nCoV12; hence, their $3CL^{pro}$ are likely homologous and have similar structures and functions. Furthermore, SARS-CoV and SARS-CoV-2 agents affect cells in the same way and employ the same protein machinery to replicate inside the host cell.

Thymidine is a precursor of nucleotides, which are important in cell metabolism and function as coenzymes. Hybridoma and myeloma cells have been reported to secrete thymidine, which exhibits high resistance to the growth inhibitory effect of thymidine. Some recent research has revealed that thymidine analogs, as well as nucleobases, are a pharmacologically diverse family, which includes cytotoxic compounds, antimicrobial agents, and immunosuppressive molecules. The antimicrobial activity of thymidine was found more promising than other nucleoside derivatives, such as uridine, cytidine, *etc.* Moreover, thymidine derivatives (*e.g.* 3′-azido-2′,3′-dideoxythymidine) showed remarkable antiviral activity and were used as prominent drug targets [19-21]. The insertions of many groups in thymidine may produce remarkable variations in biological activity and degree of selective toxicity depending on the respective chemical and physical properties [22]. The modified compounds exhibited a broad-spectrum biological activity. In the light of the above features mentioned for thymidine, this study was focused on thymidine to find potential thymidine derivatives.

Encouraged by these reports [18], the present study attempted to predict the antimicrobial efficacy of modified thymidine derivatives using several human and plant pathogens and conducting a theoretical structure-activity relationship (SAR) study. Moreover, the thermal and electrical stability and the biochemical behavior of synthesized thymidine derivatives were investigated using quantum calculations. The changes in enthalpy, free energy, dipole moment, electronic parameters (HOMO-LUMO energy gap), and surface features (MEP, DOS) were computed to study the thermodynamic and biochemical properties of the designed derivatives. Then, some chosen derivatives with better antibacterial and antifungal activity were subjected to study the molecular docking analysis

against the SARS-CoV main protease protein 1Q2W to understand their non-bonding interactions, binding mode, and binding affinity using the properties predicted by PASS. Pharmacokinetic properties were also investigated to compare the absorption, metabolism, and toxicity of the selected derivatives and study their thermodynamic, molecular orbital, MEP, and other physicochemical properties.

EXPERIMENTAL

Materials

All the solvents used in this study were of analytical grade and purified by standard procedures. All reagents used were commercially available from Sigma-Aldrich (Germany) and were used as received unless otherwise specified. Some partially protected derivatives of thymidine (2-16) (Fig. 1) were also used as test compounds. All the studied compounds were synthesized, isolated, purified, and characterized in the Lab of Carbohydrate and Nucleoside Chemistry, Department of Chemistry, University of Chittagong.

Antimicrobial Screening

The 15 modified thymidine derivatives (2-16) were used for antibacterial screening using five bacterial strains as follows: two Gram-positive strains, namely, *Bacillus subtilis* ATCC 6633 and *Staphylococcus aureus* ATCC 6538, and three Gram-negative strains, namely, *Escherichia coli* ATCC 8739, *Salmonella abony* NCTC 6017, and *Pseudomonas aeruginosa* ATCC 9027. All the compounds were dissolved in dimethylformamide (DMSO) to obtain a 2-3% solution (w/v). Then, antifungal activities of the compounds were studied against two fungi strains, namely, *Aspergillus niger* ATCC 16404 and *Aspergillus flavus* ATCC 204304. These test microorganisms (bacteria and fungi) were taken from the Department of Microbiology, University of Chittagong, Bangladesh. Disks soaked in DMSO were used as the negative control.

Screening of Antibacterial Activity

The antibacterial spectra of the tested derivatives were obtained *in vitro* by the disk diffusion method [23], and the experiments were accomplished in triplicates. The results were compared using azithromycin (Beximco Pharm. Ltd., Bangladesh) as a standard.

Minimum Inhibitory and Minimum Bactericidal Concentrations

A 96-well U-bottomed microtiter plate was used to determine the minimum inhibitory concentration (MIC) following the criteria established by the Clinical and Laboratory Standards Institute [24]. MIC was calculated as the concentration of the last well with the lowest concentration of the compound and where no bacterial accrual was found. This test revealed that the contents of the wells were seeded on plates containing Müeller-Hinton agar. Then, the minimum bactericidal concentration (MBC), which is the lowest concentration that kills bacteria, was assessed. MIC and MBC were calculated by the broth microdilution method [25].

Screening of Mycelial Growth

The *in vitro* antifungal activity of the tested derivatives was investigated by the poisoned food technique [26], in which potato dextrose agar (PDA) was used as the culture medium. The tested compounds were dissolved in DMSO to obtain a 1% (w v^{-1}) solution. A sterilized pipette was used to transfer 0.1 ml of this solution to a sterile petri dish; later, 20 ml of the medium was poured into the petri dish and allowed to solidify. The center of each petri dish was inoculated with a 5-mm mycelium block of each fungus, which was placed in the inverted position to maximize contact between the mycelium and culture medium. The mycelium block was prepared by applying a corkscrew to the growing area of a 5-day-old culture of the tested fungus growing on PDA. The inoculated plates were further incubated at 25 ± 2 °C. The experiment was conducted in triplicates, and the average of three measurements (in mm) was taken as the radial mycelial growth of the fungus. The results were compared using the antifungal agent nystatin as a standard.

Structure-activity Relationship

Structure-activity relationship (SAR) analysis was employed to predict the antimicrobial activity in the molecular frame of a pharmaceutical target. This well-known technology is often applied in the process of drug

development to guide the acquisition or synthesis of new compounds with desirable properties. In the current study, the SAR study was analyzed according to the mechanism of membrane permeation, as described by Kim [27] and Hunt [28].

PASS Predication

The online application PASS (http://www.pharmaexpert.ru/PASSonline/index.php) was employed to calculate the antimicrobial activity spectrum of the selected thymidine derivatives [29]. First, the structures of the thymidine derivatives were constructed; then, some changes were done to their SMILES rearrangement using SwissADME free online application (http://www.swissadme.ch), which is widely used to determine antimicrobial spectrum using the PASS software. This server is planned to surmise above 4000 types of antimicrobial functions together with drug and non-drug activity and suggests the best potential objects with 90% validity. PASS output was revealed by Pa (probability for active molecule) and Pi (probability for inactive molecule). The Pa and Pi scores usually vary in the range of 0.000 to 1.000, and usually, Pa + Pi ≠ 1, as these potentialities are predicted freely. Biological activities with Pa > Pi are only thought of as probable for a selected drug molecule. The results of PASS calculations were explained and used flexibly, *viz*., (i) when Pa greater than 0.7, the probability to identify the activity was analytically high, (ii) if 0.5 < Pa < 0.7, the probability to identify the activity was analytically low, suggesting that the molecule was perhaps not so alike to pharmaceutically well-established widely-used drugs, and (iii) if Pa < 0.5, the probability to identify the activity was analytically even lower than the previous level. As a result, the prediction of the spectrum of antimicrobial activity of a potential drug molecule was expressed as its intrinsic parameter.

Designing and Optimization

In computer-aided drug design, the calculation of thermal, molecular orbital, and molecular electrostatic features are widely performed by quantum mechanical methods. Geometrical calculations and subsequent alteration of all thymidine derivatives were performed using the Gaussian 09 program [30] (Fig. S1). Density functional theory (DFT), force field with Beck's (B) three-feature hybrid model [31], and Lee, Yang, and Parr's (LYP) correlation functional [32], applying the basis set 3-21G were used to conduct molecular optimization and calculate thermal and molecular properties. Initial optimization of all compounds was performed in the gas phase. The Gibbs free energy change, dipole moment, enthalpy change, heat capacity, entropy change, total energy change, and polarizability were calculated for each compound. Electronic properties, such as HOMO and LUMO, were measured using the same geometrical theory. For each thymidine derivative, the energy gap between HOMO and LUMO, molecular hardness (η), and softness (*S*) were measured from the energy values of the electronic HOMO-LUMO gap. This was done according to Parr and Pearson's explanation of DFT and Koopmans' theorem [33] on the relationship between ionization energy and electronic energy (E), on the one hand, and HOMO and LUMO energies (ε), on the other hand. The following equation was used to calculate η and *S*:

$$\eta = \frac{[\varepsilon LUMO - \varepsilon HOMO]}{2}; \quad S = \frac{1}{\eta}$$

Protein Readiness and Molecular Docking Simulation

The crystal 3D format of SARS-CoV main protease protein (pdb: 1Q2W) was recuperated in the pdb from the protein data bank [34]. PyMol software (version 1.3) was used to remove all heteroatoms and water molecules [35]. Energy minimization of the protein was performed using Swiss-PdbViewer (version 4.1.0) [36]. Furthermore, a molecular docking study against SARS-CoV main protease protein 1Q2W was conducted for all the optimized drugs. Finally, PyRx software (version 0.8) was used to carry out molecular docking simulation [37] by considering the target protein as a macromolecule and thymidine derivatives as ligands. The protein and ligands were inputted by converting the pdb format to pdbqt using MGL AutoDock Tools software. In AutoDock Vina, the grid size was maintained at 36.3196, 45.2137, and 76.4743 Å along the X, Y, and Z axes [38]. After molecular docking, the structures of both macromolecule and ligands were saved in pdbqt format. Accelrys Discovery Studio software (version 4.1)

was employed to explore the results of docking, and it predicted non-bonding interactions among thymidine derivatives and the amino acid chain of the receptor protein [39].

The validity was checked by PROCHECK online server, showing a 97.08 overall quality factors in ERRAT (http://www.ncbi.nlm.nih.gov/entrez/query.fcgi?cmd=Retrieve&db=PubMed&list_uids=8401235&dopt=Abstract) and a 96.11% score in VERIFY 3D (https://www.ncbi.nlm.nih.gov/pubmed/1853201?dopt=Abstract). Also, the PDBsum web server was used to check the sequence length (Fig. 1) and validate the main protease receptor by Ramachandran plot (Fig. S2). The results revealed that 89.6% of the residues were in the allowed region and that no residues were missing. Finally, the protein structure was checked from the protein data bank, and the following results were achieved: resolution = 1.86 Å, free R-value = 0.249, work R-value = 0.194, and observed R-value = 0.207.

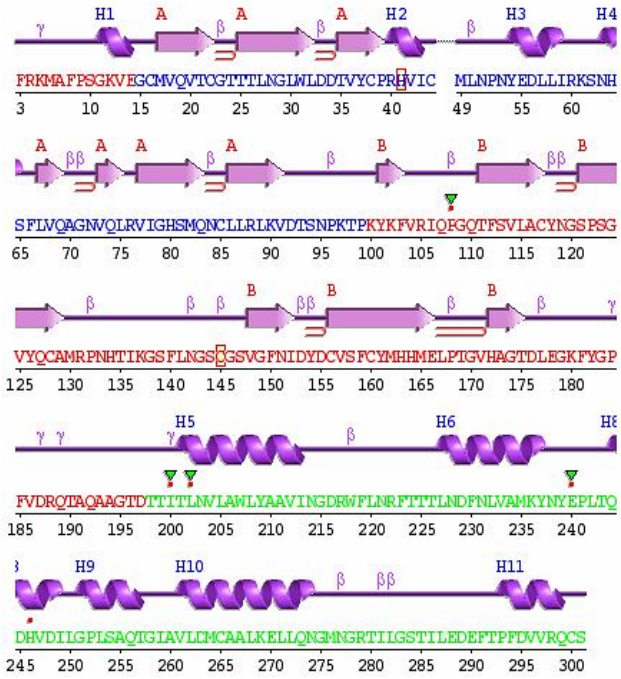

Fig. 1. Multiple sequence alignment of SARS-CoV main protease (1Q2W) produced by PDBsome with a resolution of 1.86 Å.

Docking Validation Protocol

The molecular docking validation was performed by the extraction of the co-crystallized ligand (4S-2-methyl-2,4-pentanediol) of the main protease protein (pdb: 1Q2W); then, it was re-docked into the previous position. The least energy poses gained on re-docking and the co-crystallized ligands were superimposed using PyMOL 2.3, the root mean-square deviation (RMSD) was calculated between these two superimposed molecules. The docking system was validated since the RMSD value varied in an acceptable range of 2 Å [40]. The validation of the system was performed to improve the ligand enrichment, which is considered necessary in the molecular docking method.

Pharmacokinetic Features

The online tool admetSAR was appointed to predict the pharmacokinetic activities of the designed thymidine derivatives as well as the parent compound. The online database admetSAR was examined to evaluate the pharmacokinetics profile involved in drug metabolism, toxicity, and absorption of the thymidine and its selected derivatives [41]. Using structural resemblance exploration methodology, admetSAR predicts the latest and most widespread, manually curated results for several chemicals related to acquainted absorption, distribution, metabolism, excretion, and toxicity (ADMET) profiles (21). For ADMET calculation, the admetSAR software was used, in which 96,000 sole compounds (including 45 types of ADMET-related parameters), proteins, species, and organisms are diligently curated from various sources.

Quantum Calculation

The modified thymidine derivatives studied in the present work were arranged under the reaction scheme (Fig. 2). Thymidine (1) and its derivatives (2-16) were designed and optimized as per the molecular modeling process.

Statistical Analysis

For each framework, experimental observations were displayed as mean ± standard error for three replicates. Two-tailed Student's t-tests were considered appropriate for statistical analysis, and only ρ scores less than 0.05 were considered statistically significant.

RESULTS AND DISCUSSION

In the present study, the studied derivatives (2-16) were synthesized from a known precursor, thymidine (1) (Fig. 2). These tested derivatives (2-16) may have had different types of substituents. To investigate the effectiveness of these substituents against various microorganisms, they were deliberately inserted into the 2-deoxy ribofuranose compound. Selective modification of a certain hydroxyl group is very important in nucleoside chemistry because the resulting acylation products might provide useful precursors for the synthesis of newer and bioactive products. Moreover, the designed acyl derivatives may have great effectiveness and serve as versatile intermediates for the synthesis of various NAs of fundamental importance.

Fourier Transform Infrared (FTIR) Spectroscopy

Thymidine (1) was initially treated with the unimolecular decomposition of pivaloyl chloride (Fig. 2) in dry pyridine at low temperature, followed by purification by silica gel chromatography, which yielded the pivaloyl derivative (2), as a crystalline solid (m.p.: 66-68 °C) with a yield of 78.40%. The FTIR spectrum (Fig. 3) showed carbonyl stretching absorption bands at 1690 cm^{-1} and

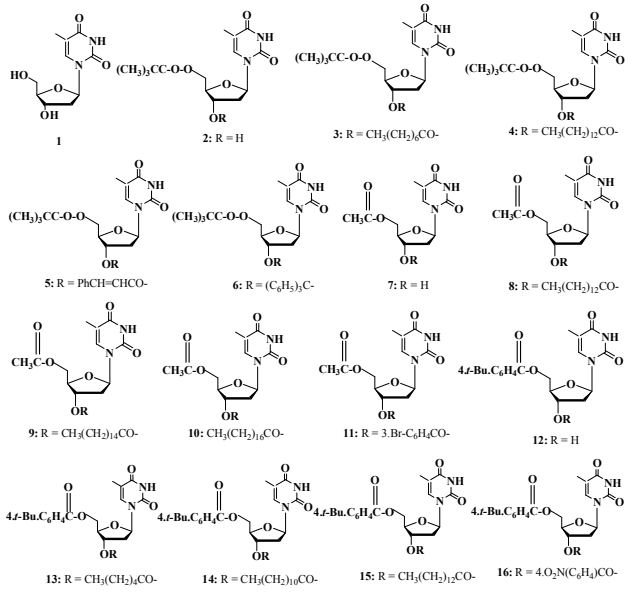

Fig. 2. The structure of the designed compounds.

hydroxyl stretching bands at 3410~3535 (br) cm^{-1}, thereby indicating the introduction of an acyl group. The mass spectrum of compound (2) had a molecular ion peak at *m/z* $[M+1]^+$ 327.31, corresponding to the $C_{14}H_{22}O_5N_2CO$ molecular formula (Table 1).

Further support for the structure corresponding to compound (2) was obtained by preparation of its octanoyl derivative (3), myristoyl derivative (4), cinnamoyl derivative (5), trityl derivative (6), acetyl derivative (7), acetyl-myristoyl derivative (8), acetyl-palmitoyl derivative (9), acetyl-stearoyl derivative (10), acetyl-3.Br.Bz derivative (11), 4-*t*-butylbenzoyl derivative (12), hexanoyl derivative (13), lauroyl derivative (14), 4-*t*-butylbenzoyl-myristoyl derivative (15), and 4-nitrobenzoyl derivative (16) in good yields (Table 1).

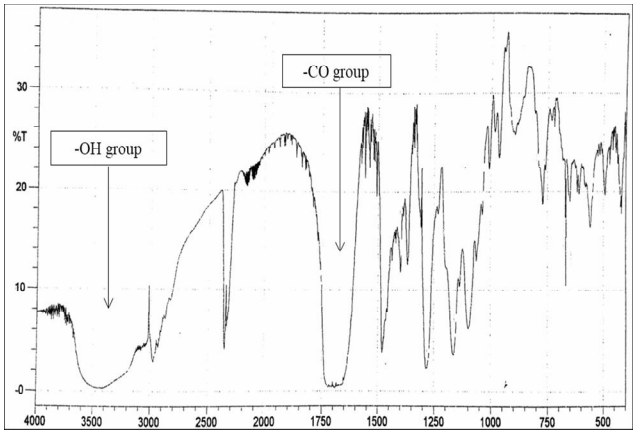

Fig. 3. The FTIR spectrum of compound 2.

2D-NMR

In the COSY spectrum of compound 2, the initial point could well be the signal from H-6a proton, which is the most downfield peak and therefore readily assigned. Thus, the signal from H-6 at the bottom left of the diagonal that has a cross-peak is labeled as H-6a, H-3′, connecting it to the signal from H-3′. H-6 proton around δ 7.31 is coupled to the hydrogen whose signal appears around δ 4.00 (*i.e.* H-3′proton). Similarly, the signal from H-3′ is further connected by a cross-peak to the signal from 3H, $(CH_3)_3CCO$- to show the coupling between H-3′ and 3H,

Table 1. FTIR, Mass, and Physicochemical Properties of the Tested Derivatives (1-16)

Compound no.	Mol. formula	FTIR (KBr, ν_{max}) cm^{-1}	LC-MS $[M+1]^+$	mp. (°C)	Yield (%)	Found (calculated)	
						%C	%H
2	$C_{14}H_{22}O_5N_2CO$	1690 (-CO), 3410~3535 (br) (-OH)	327.31	66-68	78.40	55.18 (55.16)	6.73 (6.74)
3	$C_{22}H_{36}O_6N_2CO$	1704 (C=O)	453.31	59-61	80.91	61.05 (61.02)	7.98 (7.96)
4	$C_{28}H_{48}O_6N_2CO$	1705 (C=O)	537.21	78-80	95.20	64.90 (64.89)	8.97 (8.95)
5	$C_{23}H_{28}O_6N_2CO$	1735 (C=O)	457.11	66-68	89.80	63.14 (63.11)	6.18 (6.14)
6	$C_{33}H_{36}O_5N_2CO$	1738 (-CO)	569.08	142-144	94.35	71.81 (71.79)	6.36 (6.33)
7	$C_{11}H_{16}O_5N_2CO$	1708 (C=O), 3418-3480 (br) (-OH)	285.29	58-60	90.96	50.67 (50.65)	5.66 (5.63)
8	$C_{25}H_{42}O_6N_2CO$	1701 (-CO)	495.64	69-71	97.11	63.10 (63.07)	8.52 (8.49)
9	$C_{27}H_{46}O_6N_2CO$	1710 (C=O)	523.32	88-90	77.49	64.36 (64.33)	8.84 (8.81)
10	$C_{29}H_{50}O_6N_2CO$	1711 (C=O)	551.82	77-79	93.11	65.39 (65.36)	9.10 (9.08)
11	$BrC_{18}H_{19}O_6N_2CO$	1706 (C=O)	468.28	69-71	89.75	48.80 (48.79)	4.11 (4.07)
12	$C_{20}H_{26}O_5N_2CO$	1701 (C=O), 3405-3471 (br) (-OH)	403.75	65-67	83.21	62.59 (62.57)	7.22 (7.19)
13	$C_{26}H_{36}O_6N_2CO$	1700 (C=O)	501.85	63-65	88.46	64.72 (64.69)	7.21 (7.19)
14	$C_{32}H_{48}O_6N_2CO$	1707 (C=O)	586.01	57-59	98.36	67.73 (67.72)	8.22 (8.20)
15	$C_{34}H_{52}O_6N_2CO$	1702 (C=O)	614.07	74-76	97.30	68.53 (68.51)	8.51 (8.48)
16	$C_{27}H_{29}O_8N_3CO$	1700 (C=O)	552.81	61-63	79.20	60.91 (60.89)	5.28 (5.25)

Table 2. 2D-NMR: ^{1}H NMR and ^{13}C NMR Shift Values of Compound 2

Position	δ_H (ppm) (J Hz)	(HSQC) δ_C (ppm)	HMBC
Ar-NH	9.01 (s)	129.01	H: 6,
C-6	7.31 (d, J = 2.3)	85.54	H: 1, Ar-CO
C-1′	6.32 (t, J = 6.6)	143.69	H: 6, 2
C-5′a	4.41 (dd, J = 12.0 and 4.5)	76.65	H: 3′,4′
C-5′b	4.36 (dd, J = 12.1 and 4.5)	74.95	H: 3′,4′
C-5	5.78 (d, J = 7.8)	75.49	H: 4′, CO
C-3′	4.00 (m)	91.09	H: 4, 5′a, 5′b
C-4′	3.91 (ddd, J = 3.6, 4.6 and 4.2)	71.32	H: 3′,5′a, 5′b
C-2′a	2.48(ddd, J = 13.5, 6.5 and 4.0)	103.23	H: 1, 3′
C-2′b	2.15 (ddd, J = 13.5, 6.5 and 6.7)	103.54	H: 1, 3′
$(CH_3)_3CCO$-	-	178.15	H: 5′a, 5′b

Note. ^{1}H and ^{13}C assignments were obtained from HSQC and HMBC experiments performed on Bruker DPX-400 spectrometer ($CDCl_3$, 400 MHz).

$(CH_3)_3CCO$-. The downfield shift of H-1, H-4′, H-2′, H-5′a, and H-5′b, compared to precursor compound 2 (Table 2), clearly demonstrated the attachment of pivaloyl groups at C-5′ positions. Assignment of the signals by analyzing their

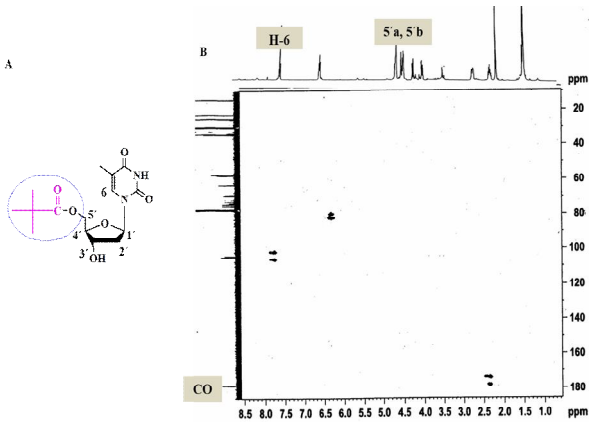

Fig. 4. HMBC spectrum of 5′-*O*-(pivaloyl)thymidine (2).

COSY, HSQC, and HMBC spectral experiments (Fig. 4), along with ^{13}C NMR spectrum, confirmed the structure as 5′-*O*-(pivaloyl)thymidine (2).

Antimicrobial Susceptibility

The results of the *in vitro* antimicrobial activity of the studied derivatives (2-16) are shown in Tables 2-4 and Fig. S3. Thymidine (1) is a vital and basic constituent of RNA, and thymidine analogs display various biological activities, such as antibacterial, antifungal, anticancer, anti-inflammatory, and DNA synthesis. Inspired by the promising role of these compounds as a therapeutic agent, these studies aimed at searching for new antimicrobial agents. In this study, thymidine analogs incorporating pivaloyl, 4-*t*-butylbenzoyl, 3-bromobenzoyl, 4-nitrobenzoyl, cinnamoyl, and fatty acid halides were synthesized as pharmacologically privileged substructures, and the thymidine derivatives were evaluated for their *in vitro* antibacterial and antifungal activity (Table 2). The standard drugs azithromycin and nystatin were used as references (positive controls) for antibacterial and antifungal assay, respectively.

Table 3. Inhibition Zone of the Studied Derivatives against Bacteria

	Diameter of inhibition zone (mm) Bacterial strains				
Entry	*B. subtilis* (+ve)	*S. aureus* (+ve)	*E.coli* (-ve)	*S. abony* (-ve)	*P. aeruginosa* (-ve)
1	NI	NI	NI	NI	NI
2	5 ± 0.21	4 ± 0.37	7 ± 0.11	4 ± 0.78	5 ± 0.65
3	NI	*18 ± 0.21	*18 ± 0.50	NI	*20 ± 0.22
4	NI	*18 ± 0.32	*20 ± 0.24	*21 ± 0.21	NI
5	10 ± 0.23	15 ± 0.26	10 ± 0.17	NI	*19 ± 0.13
6	NI	14 ± 0.30	10 ± 0.15	NI	NI
7	4 ± 0.43	6 ± 0.25	5 ± 0.54	3 ± 0.25	5 ± 0.67
8	NI	NI	10 ± 0.14	*20 ± 0.24	12 ± 0.11
9	NI	NI	NI	NI	NI
10	NI	NI	NI	NI	13 ± 0.22
11	NI	NI	10 ± 0.14	10 ± 0.16	16 ± 0.41
12	5 ± 0.32	5 ± 0.76	4 ± 0.24	5 ± 0.33	4 ± 0.26
13	NI	NI	15 ± 0.37	10 ± 0.13	15 ± 0.35
14	*22 ± 0.31	NI	*28 ± 0.41	*41 ± 0.51	10 ± 0.43
15	*24 ± 0.15	14 ± 0.40	NI	*43 ± 0.61	12 ± 0.24
16	10 ± 0.53	NI	15 ± 0.31	10 ± 0.33	NI
Azithromycin	**18 ± 0.42	**20 ± 0.22	17 ± 0.42	**19 ± 0.41	**17 ± 0.41

Note. Data are shown as mean ± SD. Values are shown for triplicate experiments. Statistically significant inhibition ($p < 0.05$) is marked with an asterisk (*) for the tested compounds and a double asterisk (**) for the reference antibiotic azithromycin; NI = No inhibition.

Table 4. MIC and MBC Data of Derivatives 3, 4, and 14 against Various Bacteria

MIC values (mg ml^{-1})					
Entry	*B. subtilis*	*S. aureus*	*E.coli*	*S. abony*	*P. aeruginosa*
3	NF	1.25 ± 0.03	0.63 ± 0.03	NF	0.32 ± 0.01
4	NF	1.25 ± 0.03	0.63 ± 0.03	0.32 ± 0.01	NF
14	0.63 ± 0.02	NF	0.32 ± 0.01	0.16 ± 0.01	NF
MBC values (mg ml^{-1})					
3	NF	2.5 ± 0.06	1.25 ± 0.06	NF	0.63 ± 0.02
4	NF	2.5 ± 0.06	1.25 ± 0.06	0.63 ± 0.02	NF
14	1.25 ± 0.04	NF	0.63 ± 0.02	0.32 ± 0.02	NF

Note. NF = Not found.

Antibacterial Inhibitory Activity

The inhibitory activity of the tested derivatives was promising against Gram-negative bacteria compared with Gram-positive bacteria (Table 3).

The acylated thymidine derivatives 3, 4, 5, 6, 14, 15, and 16 showed moderate to good inhibition against Gram-positive bacteria (Table 3, Fig. 5). The derivative 15 displayed higher inhibitory activity (24 ± 0.15 mm) against *B. subtilis* than the standard azithromycin (18 ± 0.42 mm), and derivatives 3, 4, 5, 6, and 14 showed good inhibitory activity against *S. aureus* and fair inhibition zones. However, palmitoyl derivatives, including derivative 9 (and thymidine 1 itself, demonstrated no activity against any of the tested bacteria. It can also be observed from Table 2 that derivatives 3, 4, 5, 6, 8, 11, 13, 14, and 16 exhibited moderate inhibition against Gram-negative bacteria. However, derivatives 3 (against *E. coli*), 4 (against *E. coli* and *S. abony*), 8 (against *S. abony*), and 15 (against *S. abony*) showed higher inhibitory activity than the standard drug molecule. Moreover, derivative 15 exhibited the highest inhibition zone (43 ± 0.61 mm) against *S. abony*, and derivatives 3, 4, 5, and 14 showed high inhibitory activity against both Gram-positive and Gram-negative bacteria examined in this work. The inhibition of bacterial growth was remarkable in the case of several compounds, which supports the observations in our previous reports [45].

Moreover, the results indicated that derivatives 3, 4, and 14 were effective against the tested bacteria compared with azithromycin, leading us to perform further analyses, such as the determination of MIC and MBC. The results are shown in Table 4. Derivative 14 (lauroyl derivative) had lower MIC (0.32 ± 0.01 mg ml^{-1}) and MBC (0.63 ± 0.02 mg ml^{-1}) against *E. coli* than the derivative 4, whose MIC (0.63 ± 0.03 mg ml^{-1}) and MBC (1.25 ± 0.06 mg ml^{-1}) were similar to compound 3. Furthermore, compound 14 (lauroyl derivative) exhibited lower MIC (0.16 ± 0.01 mg ml^{-1}) and MBC (0.32 ± 0.02 mg ml^{-1}) against *S. abony* than derivative 4, which exhibited an MIC of 0.32 ± 0.01 (mg ml^{-1}) and MBC of 0.63 ± 0.02 (mg ml^{-1}). In addition, derivative 14 exhibited an MIC of 0.63 ± 0.02 (mg ml^{-1}) and MBC of 1.25 ± 0.04 (mg ml^{-1}) against Gram-positive bacterium *B. subtilis*. No MIC and MBC were obtained for derivatives 3 and 4.

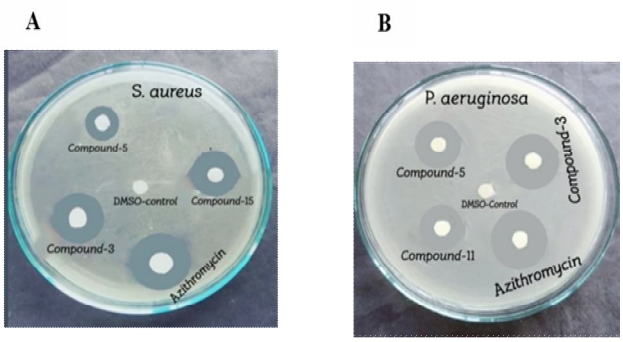

Fig. 5. Inhibition zones were observed against A) *S. cereus* by derivatives 3, 5, and 15 and B) *P. aeruginosa* by derivatives 3, 5, and 11. DMSO was treated as a negative control whereas azithromycin was treated as a positive control.

The MIC and MBC of compound 3 were found to be 0.32 ± 0.01 (mg ml^{-1}) and 0.63 ± 0.02 (mg ml^{-1}), respectively, against *P. aeruginosa* whereas the MIC and MBC of derivatives 4 and 14 were found to be zero. The MIC and MBC of compounds 3 and 4 were found to be 1.25 ± 0.03 (mg ml^{-1}) and 2.5 ± 0.06 (mg ml^{-1}), respectively, against *S. aureus*. Based on the MIC and MBC data, the derivatives can be arranged as follows: 14 > 3 = 4. Among all derivatives, derivative 14 demonstrated the most promising antibacterial activity. To the best of our knowledge, this is the first study to report the antibacterial activity of the synthesized thymidine analogs incorporating various pharmaceutically significant substructures.

Antifungal Activity

The tested compounds displayed marked toxicity against several fungal phytopathogens (Table 5 and Fig. S3). The antifungal screening data suggested that the derivatives 5 (67 ± 0.13%) and 13 (70 ± 0.10%) exhibited considerable toxicity, even higher than the standard antibiotic nystatin (66 ± 0.11%), against *A. niger*. However, interestingly, derivatives 5 (63 ± 0.35%) and 13 (59 ± 0.30%) exhibited excellent inhibitory activity, which is comparable with nystatin (63 ± 0.32%), against *A. flavus*. Moreover, derivatives 4, 10, 14, and 16 showed moderate inhibition against *A. niger* and *A. flavus*. No biological activity was found in the case of derivatives 2, 7, and 14 against both fungal pathogens.

More importantly, the incorporation of pivaloyl and 4-*t*-butylbenzoyl groups at C-5′ position and cinnamoyl and hexanoyl groups at C-3′ position, as in 3′-*O*-cinnamoyl-5′-*O*-pivaloylthymidine (5) and 5′-*O*-(4-*t*-butylbenzoyl)-3′-*O*-hexanoylthymidine (13), increased antifungal activity against *A. niger*, a finding which is consistent with our previous work. The results revealed that some of the modified acylated derivatives of thymidine may possess a wide range of antimicrobial activities. Also, the results indicated that the antimicrobial activities of thymidine derivatives were directly dependent on the type of substituent, length of the alkyl chain, and the number of acyl rings.

Computational Evaluation of Antimicrobial Activities: PASS

The PASS software was used to predict the antimicrobial spectrum of all thymidine derivatives (2-16). The PASS results are yclept as Pa and Pi (Table S1). Based on the prediction in Table S1, it can be seen that thymidine derivatives 2-16 exhibited 0.33 < Pa < 0.46 for antibacterial, 0.20 < Pa < 0.36 for antifungal, 0.55 < Pa < 0.75 for antiviral, and 0.54 < Pa < 0.84 for anti-carcinogenic effects. These results revealed that the molecules were more efficient against viruses and bacteria compared with fungal pathogens. Attachment of additional aliphatic acyl chains (C2 to C18) increased the antibacterial activity (Pa = 0.437) of thymidine (1, Pa = 0.432) whereas the insertion of -Cl and Br-substituted aromatic groups did not cause any reasonable improvement. The same scenario was observed

Table 5. Percentage of Fungal Growth Inhibition by the Tested Derivatives

	Mycelial growth inhibition (%) of fungi	
Entry	*A. niger*	*A. flavus*
1	NI	NI
2	NI	NI
3	37 ± 0.21	30 ± 0.29
4	*50 ± 0.20	48 ± 0.27
5	*67 ± 0.13	*63 ± 0.35
6	30 ± 0.21	44 ± 0.42
7	NI	NI
8	37 ± 0.14	10 ± 0.13
9	40 ± 0.21	26 ± 0.20
10	44 ± 0.43	48 ± 0.31
11	26 ± 0.23	37 ± 0.22
12	NI	NI
13	*70 ± 0.10	*59 ± 0.30
14	40 ± 0.11	37 ± 0.21
15	42 ± 0.21	36 ± 0.14
16	*52 ± 0.34	41 ± 0.11
Nystatin	**66 ± 0.11	**63 ± 0.32

Note. Data are shown as mean ± SD. Values are shown for triplicate experiments. Statistically significant inhibition ($p < 0.05$) is marked with an asterisk (*) for the tested compounds and a double asterisk (**) for the reference antibiotic nystatin. * = Good inhibition, ** = Standard antibiotic; NI = No inhibition.

for the antiviral activity of acyl chain derivatives (2-4, 7-10, and 12-15), which showed improved values compared to the halo-benzoyl derivatives (5, 6, 11, and 16). However, compound 7, which had the acetyl group, exhibited the highest antiviral activity (Pa = 0.758). We also tried to predict the anti-carcinogenic properties of these derivatives. PASS exhibited 0.54 < Pa < 0.84 for the anti-carcinogenic effect, suggesting that the thymidine derivatives had potentially more anti-carcinogenic effects than previous antimicrobial parameters. Thymidine derivatives with saturated acyl chains (2-4, 7-10, and 12-15), which showed significantly more antibacterial, antiviral, and anti-carcinogenic properties, were found more promising than the halo-benzoyl and tri-phenyl derivative (5, 6, 11, and 16) [42].

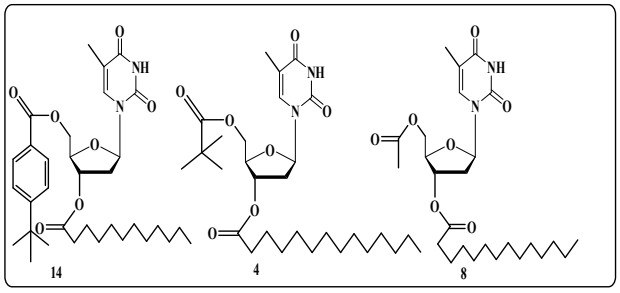

Fig. 6. SAR of derivatives 14, 4, and 8 against *S. abony* [5′-*O*-(4-*t*-butyl)-3′-*O*-lauroylthymidine (14, most active, 41 mm), 3′-*O*-myristoyl-5′-*O*-pivaloylthymidine (4, moderately active, 21 mm), 5′-*O*-acetyl-3′-*O*-myristoylthymidine 8, less active, 20 mm)].

Structure-Activity Relationship

The chemical structure and biological activity of a compound are interrelated and have received considerable attention over the past years [43]. It is clear from Tables 2 and 4 that the incorporation of lauroyl (C-12) and myristoyl (C-14) groups increased the antimicrobial potential of thymidine (1). The thymidine derivatives (2-16) were more potent against fungal than bacterial pathogens. Derivatives 3-6, 8-11, and 13-16 were found to be more active than derivatives 2, 7, and 12 against the tested pathogens. However, derivatives 2, 7, and 12 contained more hydroxyl groups; hence, they were more hydrophilic than the other compounds. Compounds having no hydroxyl groups (more hydrophobic) exhibited better antimicrobial potential than derivatives 2, 7, and 12. It can be observed from Fig. 6 that the incorporation of *t*-butyl group, benzene nucleus at C-5′ position, and lauroyl group at C-3′ position into the derivative 14 improved the antimicrobial activity (41 ± 0.51) of thymidine (1) and that derivative 14 had the highest activity due to its higher hydrophobic properties. On the other hand, the insertion of the pivaloyl group at C-5′ and C-3′ positions, containing the myristoyl group, increased the antimicrobial efficacy (21.0 mm) led to moderate inhibition against the tested pathogens. Simultaneously, derivative 8 possessed a hydrophobic methyl group and a myristoyl chain adjacent to the thymidine nucleus; accordingly, it exhibited the third-highest antibacterial activity (20.0 mm) due to lower hydrophobicity against the same bacterium *S. abony*. The inhibitory activity of the derivatives against *S. abony* can be shown in the following sequence: 14 > 4 > 8. Thus, it can be concluded that not only hydrophobicity but also the presence of an aromatic ring can increase the antibacterial activity of a compound. Additionally, it was observed that derivatives 3, 4, and 14 were highly efficient against both Gram-positive and Gram-negative bacteria.

Derivative 14, 5′-*O*-(4-*t*-butylbenzol)-3′-*O*-lauroylthymidine, was found to be more promising than other derivatives and had a higher zone of inhibition and lower MIC and MBC against *E. coli*, *B. subtilis*, and *S. abony* than the standard antibiotic azithromycin. The hydrophobicity of a compound is a crucial indicator of its biological activities, such as toxicity or alteration of membrane integrity, because it is directly connected to membrane permeation [27]. Hunt proposed that the potency of aliphatic alcohols is directly related to their lipid solubility through hydrophobic interaction between alkyl chains from alcohol and the lipid region in the membrane [28]. It is assumed that hydrophobic interactions might occur between the acyl chains of thymidine accumulated in the lipid-like structure of bacterial membranes. Due to their hydrophobic interactions, bacteria lose their membrane permeability, ultimately causing the death of bacterial pathogens [44]. This allowed us to conclude that the incorporation of 3′-*O*-lauroyl group/myristoyl in thymidine, along with 5′-*O*-4-*t*-benzoyl/lauroyl/benzoyl group, could increase the antimicrobial potential of thymidine (1).

Thermodynamic Analysis

A facile modification of chemical formation markedly influences the structural characteristic as well as thermochemical and frontier molecular orbital properties. The spontaneity of a chemical reaction and reactivity of a compound can be calculated from the theoretical Gibbs free energy change and enthalpy scores [45]. The higher is the negative scores, the higher is the thermochemical stability of a compound. In addition to that, drug development, the formation of hydrogen bonds, and nonbonded interactions are impacted by dipole moment. Theoretically, a higher dipole moment value of a molecule shows enhanced binding property [46].

The highest Gibbs free energy change (-3925.5477 Hartree), enthalpy (-3925.4575 Hartree), and electronic energy (-3925.4585Hartree) were found in derivative 11. The highest dipole moment score (8.4335 Debye) was observed in derivative 12 whereas derivative 16 exhibited the lowest dipole moment value (2.2465 Debye) (Table S2).

Frontier Molecular Orbitals

The frontier orbitals are the most vital orbitals in a molecule and are thought to reflect the chemical reactivity and kinetic stability. The frontier molecular orbitals are called HOMO and LUMO energy orbitals (Table S3).

The transition from the ground to the first excited state is associated with electronic absorption and is predominantly explained by one-electron excitation from HOMO to LUMO [47]. The kinetic stability of a molecule increases with an improvement in the HOMO-LUMO energy gap. As a result, the elimination of electrons from the ground state HOMO to the excited state LUMO needs much higher energy for excitation. Table S2 shows the calculated values of molecular orbital energies, including the two globally known chemical factors, hardness and softness, which, in this study, were calculated for all thymidine derivatives. The highest softness value was calculated for derivative 16. Also, derivative 16 exhibited an insignificant HOMO-LUMO energy gap (3.2379 eV) and hardness, suggesting that this derivative is much more reactive than other derivatives according to Pearson (35). In addition, derivative 4 showed the highest HOMO-LUMO energy gap (5.5350 eV), but it was less than that of the parent structure of thymidine molecule (1) (5.5651 eV). This clearly reveals that derivative 4 had great stability, close to that of the thymidine molecule (1). Figures S4 and S5 present the DOS curve for the maximum and minimum energy gaps of all thymidine derivatives.

In Fig. S5, the LUMO plot for derivative 4 demonstrates that the electrons are located around the myristoyl group whereas the HOMO plot indicates that the electrons are located around the thymine ring.

Molecular Electrostatic Potential

The MEP has gained attention as a reactivity factor displaying the most potential regions for the attacked electrophile and nucleophile of charged point-like reagents on organic compounds [48]. The MEP offers some explanation regarding the biological cognizance method and the H-bonding interaction [49]. The map of electrostatic potential provides an easy method to determine how different molecular geometries could interact with each other. The MEP of the selected molecule was predicted based on B3LYP with a basis set of 3-21G and optimized results (Fig. S6). MEP plays an important role in the analysis because it simultaneously shows a molecular shape and size with positive, negative, and neutral electrostatic probable areas *via* its color difference. It is also helpful in studies focused on assessing the correlation between compound structure and physicochemical parameters [50]. MEP was considered to identify the reactive zones for electrophilic and nucleophilic invasion of the optimized structure of derivatives 4, 5, 13, and 14. The potentiality of the attacking zone decreases in the order of blue > green > yellow > orange > red. The high electron density region is displayed by red color, where electrophiles can easily attack. The low electron density region is indicated by blue color, which is suitable for nucleophilic attack. Finally, the green color shows zero potential zones.

Thermophysical and physicochemical data (Table S4) indicated that among all the modified derivatives, derivative 15, which had the highest molecular weight (612.80 g mol^{-1}), exhibited the highest value for molar refractivity (174.40 $Å^3$), polarizability (377.538 a.u.), heat capacity (173.535 cal $mol^{-}kelvin^{-1}$), and entropy (285.040 cal mol $kelvin^{-1}$). This compound showed the second-highest energy value (-1990.2918 Hartree), which is less than that of derivative 11 (-3925.8557 Hartree). This

study also suggests that any improvement in the molecular weight of thymidine derivatives may increase their stability whereas the presence of bulky substituents may cause a significant increase in polarizability.

Validation of Molecular Docking

Molecular docking was performed to determine the conformation of the receptor protein-bound drug, and a re-docking of the co-crystallized ligand was performed to validate the exactness of the docking procedure. Figure S7 displays the superimposed pose between the docked ligand conformation and the co-crystallized ligand conformation. The RMSD value was found to be 1.137 Å. Gentile *et al.* [51] accomplished the re-docking of N3 peptide inhibitor against SARS-CoV-2 M^{pro} using AutoDock 4 and observed a binding score of -11.00 kcal mol^{-1}. Later, the re-docked complex was superimposed onto the co-crystallized N3-M^{pro} complex with an RMSD of 0.254 Å [52]. In the present work, the complex was allowed to interact with the same amino acid chain. Large symmetric molecules can be exchanged in the active site during docking and even the RMSD through random substitution. The reported studies exposed a new benchmark for the quality of docking poses based on visual observations. All the atoms of amino acids of both complexes were found to be superimposed without any coercion. This reveals that the use of visual inspection, as a new reference, is essential. The results partly verified the proficiency and accuracy of the docking procedure.

Figure S8 shows the LigPlot image of M^{pro} with the ligand (4S-2-methyl-2,4-pentanediol) inhibitor.

Molecular Docking

The SARS-CoV M^{pro} is one of the main enzymes in the life cycle of viruses. 2019-nCoV and SARS-CoV main proteases share 94.80% sequence identity at the amino acid level [48]. In the current study, the binding mode of thymidine and its derivatives, particularly those with better antibacterial and antifungal activities, against the SARS-CoV main protease protein (*i.e.*, 1Q2W) was investigated by molecular docking analysis (Table 6 and S5).

The analysis revealed that thymidine (1) was inactive in antibacterial and antifungal tests, with a binding affinity value of -6.9 kcal mol^{-1} to 1Q2W protein. The binding affinities of its derivatives in the ascending order were as follows: 4 < 14 < 3 < 5 < 13 < 16 (-6.0 < -6.5 < -6.7 < -7.9 < -8.1 < -8.2, kcal mol^{-1}) (Table 6). Compound 16 had the highest binding score and an additional benzene ring, which provided it with a rich density of electrons in the molecule (Fig. 7). Nonbonding interactions are often used to determine the shape and mode of docked molecules (Fig. 8). Among all the nonbonding interactions, including CH/π, CH/O, OH/π, NH/π, and CH/N, the highest drug-protein docking interaction was observed in CH/π.

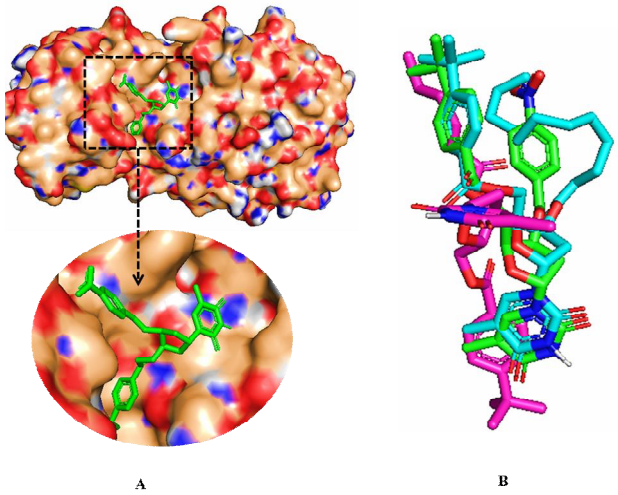

Fig. 7. Docked view of derivative 16 at the inhibitory active site of SARS-CoV M^{pro} (A); the superimposed face of all the ligands predicted from docking (B).

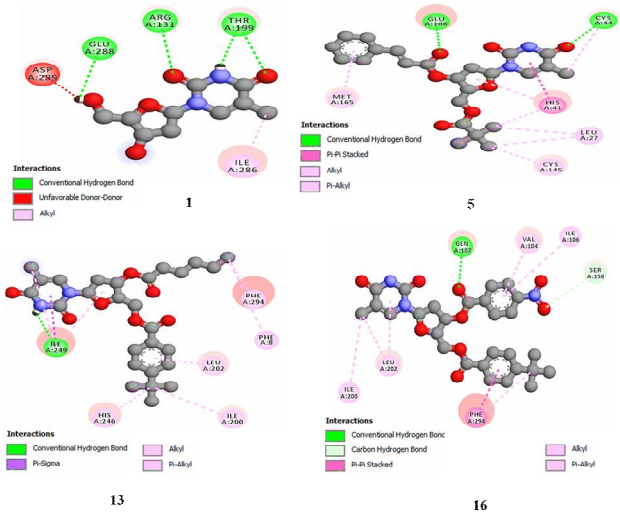

Fig. 8. Nonbonding interactions of derivatives 1, 5, 13, and 16 with the active site of SARS-CoV 1Q2W performed by Discovery Studio.

Table 6. Binding Energies (kcal mol^{-1}) and Non-Bonding Interactions of Designed Thymidine Derivatives against SARS-Cov M^{pro}

Entry	Binding affinity	Interacting contact	Types of interaction	Distance (Å)
1	-6.9	Arg131	H	2.658
		Thr199	H	2.342
		His41	H	2.272
		Glu288	H	2.391
		Ile286	A	3.832
3	-6.7	Asp187	H	2.109
		His41	H	3.078
		Cys44	H	2.260
		Met49	H	2.668
		Glu166	H	2.072
		His41	PPS	4.714
		Cys44	A	4.224
		Pro168	A	4.004
		Cys44	PA	4.818
		His41	PA	4.874
4	-6.0	Tyr54	H	2.846
		His41	PPS	4.045
		Cys44	A	4.052
		Cys44	PA	5.465
		His41	PA	4.893
5	-7.9	Cys44	H	2.455
		Glu166	H	2.341
		His41	PPS	3.937
		Cys44	A	4.136
		Met165	PA	5.129
		His41	PA	4.967
13	-8.1	Ile249	H	3.093
		Ile249	PSi	3.562
		Ile249	A	5.093
		Ile286	A	5.374
		Ile249	A	4.248
		Leu202	PA	5.040
		Phe8	PA	4.908
		His246	PA	4.676
		Phe294	PA	4.485
14	-6.5	Gln107	H	1.864
		Gln110	C	3.710
		His41	C	3.652
		Phe294	PPS	3.828
		Val104	A	3.581
		Leu202	A	4.683
		Leu202	PA	5.305
		Phe294	PA	4.337
16	-8.2	Gln107	H	2.211
		Ser158	C	3.729
		Phe294	PPS	3.772
		Ile200	A	4.984
		Leu202	A	4.505
		Val104	PA	5.384
		Ile106	PA	5.494
		Leu202	PA	5.392
		Phe294	PA	4.292
Remdesivir	-9.7	Ile200	A	5.102
		Leu202	PA	5.094
		Cys44	PA	3.661
		Pro132	PA	4.047
		His246	PA	4.382

Note. C = Carbon–hydrogen bond, A = alkyl, PPS = Pi–Pi stacked, H = Conventional hydrogen bond, PA = Pi–alkyl, Psi = Pi Sigma, Asp = Aspartic acid, Glu = Glutamic acid, Leu = Leucine, Thr = Threonine, Gln = Glutamine, Phe = Phenylalanine, Ile = Isoleucine, Arg = Arginine, Val = Valine, Ser = Serine, Pro = Proline, Tyr = Tyrosine, His = Histidine, Cys = Cysteine, Met = Methionine.

Parent molecule thymidine (1) exhibited interactions with the histidine minutiae of the protein and a sharp interaction within a closer bond distance (2.272 Å). Although arginine, threonine, and glutamic acid interactions were found, threonine resulted in a shorter bond distance (2.34224 Å) due to the unique interaction of the branched alkyl chain with the thymine ring. In comparison with parent ligand 1, derivative 3, similar to alkyl, π-Alkyl, and π–π stacked, mainly showed hydrophobic bonding, most of its interactions with cysteine were in a shorter bond distance (2.260 Å). As regards derivatives 4 and 5, shorter bond distance interactions were observed for tyrosine, glutamic acid, and cysteine because the structural fulfillment of these two derivatives allowed small amino acids to the vicinity of the neighboring drug moiety. On the other hand, different types of significant hydrophobic molecular interactions, such as π-π sigma, π-π stacked, π-alkyl, and carbon-

hydrogen, were observed derivatives 13, 14, and 16. These three compounds exhibited prominent interactions with isoleucine, leucine, glutamine, and phenylalanine moiety at a very close distance. Binding energy and binding mode of interaction were improved in derivatives 5, 13, and 16 because of significant hydrogen bonding interactions. It was also observed that the changes in the -OH group in thymidine strengthened the π-π interactions with the amino acid chain on the binding site whereas the increase in their polarity resulted in the formation of hydrogen bond interactions. The maximum numbers of H-bonds were observed for derivative 3, with Asp187, His41, Cys44, Met49, and Glu166 residues. Most interestingly, derivatives 3 and 5 showed two identical hydrogen bonds with the chains Cys44 and Glu166. On the other hand, derivatives 14 and 16 had similar H-bond interactions with Gln107, irrespective of different bonding distances. Moreover, derivatives 4 and 13 were found to have H-bonds with two different residues, namely, tyr54 and Ile254. Remdesivir is a well-known anti-covid drug used in this study as a standard. Similar to synthesis compounds, Remdesivir also showed a similar binding site (Ile200, Leu202, Cys44, and His246) through the alkyl and pi-alkyl bond. The results revealed that the analyzed thymidine derivatives, similar to the standard drug Remdesivir, bound within the active site of the main protease of SARS-CoV, which is crucial in preventing the protein mutarotation of the virus by minimizing the viral replication. In molecular docking exploration, some prime and common residues of SARS-CoV 1Q2W with active sites were His41, Cys44, Phe294, and Leu202, predicting several nonbonding interactions with drug molecules (Table 5 and Fig. 7).

It has already been reported that ten commercial medicines can possibly form H-bonds with key residues of 2019-nCoV main protease [53]. Hydrogen-bonds usually play a major role in shaping the specificity of ligand binding with the protein, drug design in biochemical processes, molecular recognition, and biological activity. The H-bond and hydrophobic maps of derivative 16 are illustrated in Figs. S9 and S10. Although derivative 9 showed mostly hydrogen-type nonbonding interactions, it had a significant range of hydrophobicity due to the presence of aromatic rings.

Pharmacokinetic Analysis

Pharmacokinetic properties were also calculated to evaluate the metabolism, absorption, and toxicity of the designed thymidine derivatives. AdmetSAR calculation (Table S6) predicted that the tested thymidine derivatives were non-carcinogenic and had category III oral toxicity. Therefore, it can be stated that thymidine derivatives are comparatively innoxious for oral application. All derivatives were P-glycoprotein non-inhibitors. P-glycoprotein inhibitors can obstruct the absorption, permeability, and retention of the drug. All the molecules indicated permeability through the blood-brain barrier.

CONCLUSIONS

In this investigation, several tested derivatives showed promising antimicrobial activity. The best inhibitory activity was observed against Gram-negative bacteria. *S. abony*, E. coli, and P. aeruginosa, among Gram-negative bacteria, and *S. aureus*, among Gram-positive bacteria, were found to be the most susceptible pathogens. Hence, the acylated derivatives of thymidine (2-16) can be considered as a probable source for the development of newer and better antimicrobial candidates against several pathogenic organisms. The properties of the thymidine derivatives 2-16 predicted by PASS were Pa < 0.46 for antibacterial, Pa < 0.36 for antifungal, Pa < 0.75 for antiviral, and Pa < 0.84 in anti-carcinogenic properties, which reveals the antimicrobial potency of the modified derivatives. Furthermore, the molecular docked complex of derivatives 13 and 16 and SARS-CoV M^{pro} 1Q2W exhibited comparatively better binding scores, with significant nonbonding interactions compared to the parent ligand. The molecular docking validation clearly showed that the RMSD values were in the standard range. The ADMET properties showed a promising result for *in silico* properties, suggesting that all the modified compounds had an improved pharmacokinetic profile. Since the studied compounds possess antibacterial and antifungal properties, they have the potential to exert antiviral effects as well. This work may be helpful in assessing the chemical, thermal, biological, physicochemical, and pharmacological properties of ribofuranose-modified thymidine derivatives.

ACKNOWLEDGEMENTS

The authors are grateful to the Ministry of Science and Technology (MOST), Government of the People's Republic of Bangladesh, for providing financial support (Ref.: 39.00.0000.09.14.009.2019/Phy's-32/502) for this research.

Declaration of Interest

The authors declare no conflict of interest.

Author Contributions: A.A., K.M.R., and A.A. carried out design and molecular docking studies, and S.D. performed the antimicrobial study. B.B. contributed to the editing, and S.M.A.K. supervised and contributed to the writing and editing of the manuscript. All authors approved the final version of the manuscript.

REFERENCES

[1] Meanwell, M.; Silverman, S. M.; Lehmann, J.; Adluri, B.; Wang, Y.; Cohen, R.; Campeau, L. -C.; Britton, R., A short de novo synthesis of nucleoside analogs. *Science*, **2020**, *369*, 725-730, DOI: 10.1126/science.abb3231.

[2] Guinan, M.; Benckendorff, C.; Smith, M.; Miller, G. J., Recent advances in the chemical synthesis and evaluation of anticancer nucleoside analogues. *Molecules*, **2020**, *25*, 2050-2075, DOI: 10.3390/molecules25092050.

[3] Jordheim, L. P.; Durantel, D.; Zoulim, F.; Dumontet, C., Advances in the development of nucleoside and nucleotide analogues for cancer and viral diseases. *Nat. Rev. Drug Discov.* **2013**, *12*, 447-464, DOI: 10.1038/nrd4010.

[4] Taylor, R.; Kotian, P.; Warren, T.; Panchal, R.; Bavari, S.; Julander, J.; S. Dobo, A.; Rose, Y.; ElKattan, B.; Taubenheim, Y.; Babu, W. P., Sheridan. BCX4430-A broad-spectrum antiviral adenosine nucleoside analog under development for the treatment of Ebola virus disease. *J. Infec. Public Health.* **2016**, *9*, 220–226, DOI: 10.1016/j.jiph.2016.04.002.

[5] Pillai, K.; Pilay, V.; Jasamai, M.; Thayan, R.; Santhanam, J.; Hassan, S. S.; Yap, W. B., Nucleoside analogs as potential antiviral agents for dengue virus infections. *Med. Chem. Res.* **2017**, *26*, 1382-1387, DOI: 10.1007/s00044-017-1863-4.

[6] Eyer, L.; Nencka, R.; Huvarová, I.; Palus, M.; Alves, M. J.; Gould, E. A.; Clercq, E. D.; Růžek, D., Nucleoside inhibitors of Zika virus. *J. Infec. Disease*, **2016**, *214*, 707-711, DOI: 10.1093/infdis/jiw226.

[7] Hamuy, R.; Berman, B., Topical antiviral agents for herpes simplex virus infections. *Drugs Today*, **1998**, *34*, 1013-1025, DOI: 10.1358/dot.1998.34.12.487486.

[8] Rabasseda, X., Brivudine: A herpes virostatic with rapid antiviral activity and once-daily dosing. *Drugs Today*. **2003**, *39*, 359-371, DOI: 10.1358/dot.2003.39.5.740221.

[9] Yuen, G. J.; Weller, S.; Pakes, G. E., A review of the pharmacokinetics of abacavir. *Clin. Pharmacokinetics*, **2008**, *47*, 351-371, DOI: 10.2165/00003088-200847060-00001.

[10] Ching, L. L.; Edward, G.; Yun, F. L.; Nathaniel, W. H.; Chao, T.; Satawat, W.; Yuming, C.; Yagang, E. J.; Heathcote, J.; Rasenack, B.; Natalie, V. N.; Nikolai, M. D. B.; Adrian, Z.; Stefan, M. M.; Young, G.; Zachary, C.; George, F. C.; Barbara, A. B., Nathaniel Telbivudine *versus* Lamivudine in patients with Chronic Hepatitis B. *New Eng. J. Med.* **2007**, *357*, 2576-2588, DOI: 10.1056/NEJMoa066422.

[11] Shealy, Y. F.; O'Dell, C. A.; Shannon, W. M.; Arnett, G., Carbocyclic analogs of 5-substituted uracil nucleosides. Synthesis and antiviral activity. *J. Med. Chem.* **1983**, *26*, 156-161, DOI: org/10.1021/jm00356a008.

[12] Hurst, M.; Noble, S., Stavudine: An update of its use in the treatment of HIV infection. *Infec. Drugs.***1999**, *58*, 919-949, DOI: 10.2165/00003495-199958050-00012.

[13] Amin, M. R.; Yasmin, F.; Hosen, M. A.; Dey, S.; Mahmud, S.; Saleh, M. A.; Emran, T. B.; Hasan, I.; Fujii, Y.; Yamada, M.; Ozeki, Y.; Kawsar, S. M. A., Synthesis, antimicrobial, anticancer, PASS, molecular docking, molecular dynamic simulations and pharmacokinetic predictions of some methyl β-D-galactopyranoside analogs**.** *Molecules*, **2021**, *26*, 1-25, DOI: 10.3390/molecules26227016.

[14] Spellberg, B.; Guidos, R.; Gilbert, D.; Bradley, J.; Boucher, H. W.; Scheld, W. M.; Bartlett, J. G.; Edwards, J., The epidemic of antibiotic-resistant

infections: A call to action for the medical community from the infectious diseases society of america. *Clin. Infec. Diseases*, **2008**, *46*, 155-164, DOI: 10.1086/524891.

[15] Kawsar, S. M. A.; Faruk, M. O.; Rahman, M. S.; Fujii, Y.; Ozeki, Y., Regioselective synthesis, characterization, and antimicrobial activities of some new monosaccharide derivatives. *Scientia Pharm*. **2014**, *82*, 1-20, DOI: 10.3797/scipharm.1308-03.

[16] Lu, H., Drug treatment options for the 2019-new coronavirus (2019-nCoV). *Bioscience Trends*. **2020**, *14*, 69-71, DOI: 10.5582/bst.2020.01020.

[17] Maowa, J.; Hosen, M. A.; Alam, A.; Rana, K. M.; Fujii, Y.; Ozeki, Y.; Kawsar, S. M. A., Pharmacokinetics and molecular docking studies of uridine derivatives as SARS-COV-2 Mpro Inhibitors. *Phys. Chem. Res*. **2021**, *9*, 385-412, DOI: 10.22036/pcr.2021.264541.1869.

[18] Rana, K. M.; Maowa, J.; Alam, A.; Dey, S.; Hosen, A.; Hasan, I.; Fujii, Y.; Ozeki, Y.; Kawsar, S. M. A., In silico DFT study, molecular docking, and ADMET predictions of cytidine analogs with antimicrobial and anticancer properties. *In Silico Pharmacol*. **2021**, *9*, 1-24, DOI: 10.1007/s40203-021-00102-0.

[19] Alam, A.; Hosen, M. A.; Hosen, A.; Fujii, Y.; Ozeki, Y.; Kawsar, S. M. A., Synthesis, characterization, and molecular docking against a receptor protein FimH of Escherichia coli (4XO8) of thymidine derivatives. *J. Mex. Chem. Soc*. **2021**, *65*, 256-276. DOI: 10.29356/jmcs.v65i1.1464.

[20] Devi, S. R.; Jesmin, S.; Rahman, M.; Manchur, M. A.; Fujii, Y.; Kanaly, R. A.; Ozeki, Y.; Kawsar, S. M. A., Microbial efficacy and two step synthesis of uridine derivatives with spectral characterization. *ACTA Pharm. Sci*. **2019**, *57*, 47-68. DOI: 10.23893/1307-2080.APS.05704.

[21] Hosen, M. A.; Alam, A.; Islam, M.; Fujii, Y.; Ozeki, Y.; Kawsar, S. M. A., Geometrical optimization, PASS prediction, molecular docking, and *in silico* ADMET studies of thymidine derivatives against FimH adhesin of Escherichia coli. *Bulg. Chem. Commun*. **2021**, *53*, 327-342. DOI: 10.34049/bcc.53.3.5375.

[22] Kawsar, S. M. A.; Hosen, M. A., An optimization and pharmacokinetic studies of some thymidine derivatives. *Turkish Comp. Theo. Chem*. **2020**, *4*, 59-66. DOI: 10.33435/tcandtc.718807.

[23] Bauer, A. W.; Kirby, W. M. M.; Sherris, J. C.; Turck, M., Antibiotic susceptibility testing by a standardized single disk method. *American J. Clin. Pathol*. **1966**, *45*, 493-496, DOI: 10.1093/ajcp/45.4_ts.493.

[24] Clinical and Laboratory Standards Institute (CLSI). Performance Standards for Antimicrobial Disk Susceptibility Tests. 23rd informational Supplement M100-S23, Wayne, USA, **2013**.

[25] Nickolai, D. J.; Lammel, C. J.; Byford, B. A.; Morris, J. H.; Kaplan, E. B.; Hadley, W. K.; Brooks, G. F., Effects of storage temperature and pH on the stability of eleven beta-lactam antibiotics in MIC trays. *J. Clin. Microbiol.* **1985**, *21*, 366-370, DOI: 10.1128/jcm.21.3.366-370.1985.

[26] Grover, R. K.; Moore, J. D., *In vitro* efficacy of certain essential oils and plant extracts against three major pathogens of Jatropha curcas L. *Phytopathology*, **1962**, *52*, 876-879, DOI: 10.4236/jqis.2011.12006.

[27] Kim, Y. M.; Farrah, S.; Baney, R. H., Structure-antimicrobial activity relationship for silanols, a new class of disinfectants, compared with alcohols and phenols. *Int. J. Antimicrob. Agents.* **2007**, *29*, 217-222, DOI: 10.1016/j.ijantimicag.2006.08.036.

[28] Hunt, W. A., The effects of aliphatic alcohols on the biophysical and biochemical correlates of membrane function. *Adv. Exp. Med. Biol*. **1975**, *56*, 195-210, DOI: 10.1007/978-1-4684-7529-6_9.

[29] Kumaresan, S.; Senthilkumar, V.; Stephen, A.; Balakumar, B. S., GC-MS analysis and PASS-assisted prediction of biological activity spectra of extract of Phomopsis sp. Isolated from Andrographis paniculata. *World J. Pharm. Res*. **2015**, *4*, 1035-1053. DOI: ?

[30] Frisch, M. J.; Trucks, G. W.; Schlegel, H. B.; Scuseria, G. E.; Robb, A.; Cheeseman, J. R.; Scalmani, G.; Barone, V.; Mennucci, M.; Petersson G. A.; *et al*., Gaussian 09. Gaussian Inc, Wallingford, CT, **2009**, https://gaussian.com/g09citation/.

[31] Becke, A. D., Density-functional exchange-energy approximation with correct asymptotic behaviour. *Phys. Rev.A*. **1988**, *38*, 3098-3100, DOI: 10.1103/PhysRevA.38.3098.

[32] Lee, C.; Yang, W.; Parr, R. G., Development of the colle-Salvetti correlation-energy formula into a

functional of the electron density. *Phys. Rev. B.* **1988**, *37*, 785-789, DOI: 10.1103/PhysRevB.37.785.

[33] Pearson, R. G., Absolute electronegativity and hardness correlated with molecular orbital theory. *Proc. Natl. Acad. Sci. U. S. A.* **1986**, *83*, 8440-8441, DOI: 10.1073/pnas.83.22.8440.

[34] Berman, H. M.; Westbrook, J.; Feng, Z.; Gilliland, G.; Bhat, T. N.; Weissig, H.; Shindyalov, I. N.; Bourne, P. E., The protein data bank. *Nucleic Acids Res.* **2000**, *28*, 235-242, DOI: 10.1093/nar/28.1.23.

[35] Delano, W. L., The PyMOL Molecular Graphics System. De-Lano Scientific, San Carlos, CA, USA, **2002**.

[36] Guex, N.; Peitsch, M. C., SWISS-MODEL and the Swiss-PdbViewer: an environment for comparative protein modeling. *Electrophoresis*, **1997**, *18*, 2714-2723, DOI: 10.1002/elps.1150181505.

[37] Williams, C. H.; Hong, C. C., (Eds.). Chemical Biology: Methods and Protocols. Springer, New York USA, **2015**, 243-250, DOI: 10.1007/978-1-4939-2269-7.

[38] Dallakyan, S.; Olson, A. J., Small-molecule Library Screening by Docking with PyRx. Chemical Biology. Springer, New York USA, **2015**, pp. 243-250.

[39] Version ADS 4.0. Accelrys, San Diego, USA, **2017**.

[40] Onodera, K.; Satou, K.; Hirota, H., Evaluations of molecular docking programs for virtual screening. *J. Chem. Inform. Model.* **2007**, *47*, 1609-1618, DOI: 10.1021/ci7000378.

[41] Cheng, F.; Li, W.; Zhou, Y.; Shen, J.; Wu, Z.; Liu, G.; Lee, P. W.; Tang, Y., admetSAR: A comprehensive source and free tool for assessment of chemical ADMET properties. *J. Chem. Inform. Model.* **2012**, *52*, 3099-3105, DOI: 10.1021/ci300367a.

[42] Lagunin, A.; Zakharov, A.; Filimonov, D.; Poroikov, V., QSAR modelling of rat acute toxicity on the basis of PASS prediction. *Mol. Inform.* **2011**, *30*, 241-250, DOI: 10.1002/minf.201000151.

[43] Huseyin, C.; Murat, S.; Murat, G.; Serdar, D.; Gulru, K.; Claudiu, T. S.; Deniz, E., Inhibition of acetylcholinesterase and butyrylcholinesterase with uracil derivatives: kinetic and computational studies. *J. Enzyme Inhibition Med. Chem.* **2019**, *34*, 429-437, DOI: 10.1080/14756366.2018.1543288.

[44] Judge, V.; Narasimhan, B.; Ahuja, M.; Sriram, D.; Yogeeswari, P.; Clercq, E. D.; Pannecouque, C., Synthesis, antimycobacterial, antiviral, antimicrobial activity and QSAR Studies of N2-acyl isonicotinic acid hydrazide derivatives. *J. Balzarini Med. Chem.* **2013**, *9*, 53-76, DOI: 10.2174/157340613804488404.

[45] Cohen, N.; Benson, S. W., Estimation of heats of formation of organic compounds by additivity methods. *Chem. Rev.* **1993**, *93*, 2419-2438, DOI: 10.1021/cr00023a005.

[46] Lien, E. J.; Guo, Z. R.; Li, R. L.; Su, C. T., Use of dipole moment as a parameter in drug-receptor interaction and quantitative structure-activity relationship studies. *J. Pharm. Sci.* **1982**, *71*, 641-655, DOI: 10.1002/jps.2600710611.

[47] Saravanan, S.; Balachandran, V., Quantum chemical studies, natural bond orbital analysis and thermodynamic function of 2,5-dichlorophenyl-isocyanate. *Spectrochim. Acta Part A: Mol. Biomol. Spectros.* **2014**, *120*, 351-364, DOI: 10.1016/j.saa.2013.10.042.

[48] Amin, M. L., P-glycoprotein inhibition for optimal drug delivery. *Drug Target Insights.* **2013**, *7*, 27-34, DOI: 10.4137/DTI.S12519.

[49] Politzer, P.; Murray, J. S., Molecular electrostatic potentials and chemical reactivity. *Rev. Comput. Chem.* **1991**, *2*, 273-312, DOI: 10.1002/wcms.1326.

[50] Politzer, P.; Truhlar, D. G., (Eds.). Chemical Applications of Atomic and Molecular Electrostatic Potentials. Reactivity, Structure, Scattering, and Energetics of Organic, Inorganic, and Biological Systems. Springer, DOI: https://www.springer.com/gp/book/9780306406577.

[51] Gentile, D.; Scala, A.; Sciortino, M. T.; Piperno, A.; Rescifina, A., Putative inhibitors of SARS-CoV-2 main protease from A library of marine natural products: A virtual screening and molecular modeling study. *Marine Drugs.* **2020**, *18*, 225-244, DOI: 10.3390/md18040225.

[52] Serseg, T.; Benarous, K.; Yousfi, M., Hispidin and lepidine E: two natural compounds and folic acid as potential inhibitors of 2019-novel coronavirus main protease (2019-nCoVMpro), molecular docking and SAR study. *Curr. Comput. Aided Drug Des.* **2021**, *17*,

469-479, DOI: 10.2174/1573409916666200422075440.
[53] Liu, X.; Wang, X. J., Potential inhibitors against 2019-nCoV coronavirus M protease from clinically approved medicines. *J. Genet. Genom.***2020**, *47*, 119-121, DOI: 10.1016/j.jgg.2020.02.001.